

STePAR: an automatic code to infer stellar atmospheric parameters

H. M. Tabernero¹, E. Marfil², D. Montes², and J. I. González Hernández^{3,4}

¹ Centro de Astrobiología (CSIC-INTA), Carretera de Ajalvir km 4, Torrejón de Ardoz, 28850 Madrid, Spain
e-mail: htabernero@cab.inta-csic.es

² Departamento de Física de la Tierra y Astrofísica & IPARCOS-UCM (Instituto de Física de Partículas y del Cosmos de la UCM),
Facultad de Ciencias Físicas, Universidad Complutense de Madrid, 28040 Madrid, Spain

³ Instituto de Astrofísica de Canarias (IAC), 38205 La Laguna, Tenerife, Spain

⁴ Universidad de La Laguna (ULL), Departamento de Astrofísica, 38206 La Laguna, Tenerife, Spain

Received 14 March 2019 / Accepted dd mm 2019

ABSTRACT

Context. STePAR is an automatic code written in Python 3.X designed to compute the stellar atmospheric parameters T_{eff} , $\log g$, $[\text{Fe}/\text{H}]$, and ξ of FGK-type stars by means of the *EW* method. This code has already been extensively tested in different spectroscopic studies of FGK-type stars with several spectrographs and against myriads of Gaia-ESO Survey UVES U580 spectra of late-type, low-mass stars as one of its thirteen pipelines.

Aims. We describe the code and test it against a library of well characterised Gaia benchmark stars. We also release the code to the community and provide the link for download.

Methods. We carried out the required *EW* determination of Fe I and Fe II spectral lines using the automatic tool TAME. STePAR implements a grid of MARCS model atmospheres and the MOOG radiative transfer code to compute stellar atmospheric parameters by means of a Downhill Simplex minimisation algorithm.

Results. We show the results of the benchmark star test and also discuss the limitations of the *EW* method, and hence the code. In addition, we found a small internal scatter for the benchmark stars of 9 ± 32 K in T_{eff} , 0.00 ± 0.07 dex in $\log g$, and 0.00 ± 0.03 dex in $[\text{Fe}/\text{H}]$. Finally, we advise against using STePAR on double-lined spectroscopic binaries or spectra with $R < 30,000$, $\text{SNR} < 20$ or $v \sin i > 15$ km s⁻¹ as well as stars later than K4 or earlier than F6.

Key words. techniques: spectroscopic – methods: data analysis – stars: fundamental parameters

1. Introduction

The characterization of stellar spectra is a matter of utmost importance to several fields in modern astrophysics. It provides for the study and better understanding of the different constituents of our galaxy in terms of both individual and large-scale properties of target objects.

For this reason, stellar spectroscopy stands as a powerful tool that is being widely used in observational surveys, both ongoing and underway, such as the APO Galactic Evolution Experiment (APOGEE, Dawson et al. 2013), the GALactic Archeology with HERMES (GALAH, De Silva et al. 2015), the LAMOST Experiment for Galactic Understanding and Exploration (LEGUE, Deng et al. 2012), the RADial Velocity Experiment (RAVE, Kunder et al. 2017), the Sloan Extension for Galactic Understanding and Exploration (SEGUE, Lee et al. 2008), the Gaia-ESO Survey (GES, Gilmore et al. 2012), and WEAVE (Dalton et al. 2018).

Such large surveys have especially been designed to yield full sets of stellar parameters for as many stars as possible by means of automated methods that ensure the homogeneity of the results. These parameters include the effective temperature, T_{eff} ; the surface gravity, $\log g$; the metallicity, $[\text{M}/\text{H}]$; and the microturbulent velocity, ξ .

In this regard, late-type, low-mass stars of FGK spectral types remain one of the most interesting targets on account of their ubiquity. Furthermore, the optical spectra of these stars have plenty of iron features that are very sensitive to the stellar atmospheric parameters.

The computation of stellar atmospheric parameters of FGK stars under spectroscopic scrutiny is often carried out by means of two different methods: the spectral synthesis method and the *EW* method. The former uses theoretical synthetic spectra in order to find the best match to a target observed spectrum, whereas the latter uses the strength of several spectral lines to find the set of stellar atmospheric parameters that best reproduce the measured *EW*s. Thorough, recent reviews of these techniques can be found in Allende Prieto (2016), Nissen & Gustafsson (2018), Jofré et al. (2018), and Blanco-Cuaresma (2019).

There are many implementations of these two methods that are publicly available to the community. Among the spectral synthesis implementations stand the APOGEE pipeline (AS-CAP, García Pérez et al. 2016), and Spectroscopy Made Easy (SME, Piskunov & Valenti 2017; Valenti & Piskunov 1996), whereas the *EW* method is implemented in tools such as FAMA (Magrini et al. 2013), GALA (Mucciarelli et al. 2013), BACHUS (Masseron et al. 2016), and SPECIES (Soto & Jenkins 2018). Remarkably, there are also general-purpose toolkits such as the integrated Spectroscopic framework (iSpec, see Blanco-Cuaresma et al. 2014a) and FASMA (Andreasen et al. 2017; Tsantaki et al. 2018) that can compute the stellar atmospheric parameters of any given star under both methods.

In general, spectral synthesis methods are based on a χ^2 minimization algorithm based on a precomputed grid of atmospheric models (see Valenti & Piskunov 1996; García Pérez et al. 2016; Tsantaki et al. 2018). The theoretical spectra, which may sometimes be split up into spectral regions of interest (see e.g. Tsan-

arXiv:1907.06512v1 [astro-ph.SR] 15 Jul 2019

taki et al. 2014), are finally compared with the observations to find the atmospheric model that best fits the data. This approach can also be found in González Hernández et al. (2004) and Al-lende Prieto et al. (2006).

On the other hand, the *EW* method employs the standard technique based on the iron ionization and excitation balance, taking advantage of the high sensitivity of the strength (i.e. the *EW*) of Fe I and Fe II lines to the variation of the stellar atmospheric parameters. This approach rests on the curves of growth that link, by means of the Saha and Boltzmann equations, the observed *EW* to the column density of the chemical species that causes the line in the stellar spectrum. Further details on these two equations can be found in e.g. Hubeny & Mihalas (2014). This method has already been applied to several studies found in the literature (see e.g. Ghezzi et al. 2010; Santos et al. 2004; Sousa et al. 2008).

The required *EW* determination of the Fe lines can be carried out either automatically or manually. There are some automatic tools designed for this task, such as ARES (Sousa et al. 2007), DAOSPEC (Stetson & Pancino 2008), and TAME (Kang & Lee 2012). All these tools accept some input parameters that can be fine-tuned depending on the quality of the target spectrum under analysis (i.e. the position of the stellar pseudo-continuum, the list of spectral lines to be measured, the parameters that constrain the detection of spectral lines according to the spectral resolution, and so on). In this regard, we highlight the fact that any given linelist is generally assembled from the analysis of a template star (usually the Sun, e.g. Santos et al. 2004; Sousa et al. 2008). However, in some cases the template star may be different, e.g. a cool, K-type star (Tsantaki et al. 2013), or a giant star (Hekker & Meléndez 2007). The selected lines must be as unblended as possible to avoid the contamination of neighbouring lines that could potentially affect the *EW* measurements.

In this work we present a full description of the automatic code STEPAR, written in Python 3.X, which is based on the *EW* method. This code has already been applied to the careful study of FGK-type stars (González Hernández et al. 2012; Taberero et al. 2012; Taberero 2014; Taberero et al. 2017; Jofré et al. 2017; Montes et al. 2018) and has also been extensively used to automatically analyse hundreds of Gaia-ESO UVES spectra since it stands as one of the thirteen pipelines that characterises the UVES U580 spectra of late-type, low-mass stars (see Smiljanic et al. 2014; Lanzafame et al. 2015).

A concise description of the complete method is found in Sect. 2. Detailed explanations of the STEPAR internal workflow are given in Sect. 3. In Sect. 4 we discuss our results and compare them to those obtained in previous works, as well as to evolutionary tracks. Finally, in Sect. 5 we warn of the limitations of the *EW* method, and hence STEPAR.

2. The STEPAR code

The basic ingredients that STEPAR needs to derive the stellar atmospheric parameters T_{eff} , $\log g$, $[\text{Fe}/\text{H}]$, and ξ , fully explained in Sect. 2.1, are the following:

- (i) A grid of stellar atmospheric models: MARCS model atmospheres (Gustafsson et al. 2008).
- (ii) A code to solve the radiative transfer problem under the assumption of local thermodynamic equilibrium (LTE): the MOOG code (Snedden 1973).
- (iii) A list of Fe I and Fe II spectral lines along with their atomic parameters.
- (iv) A programme to measure the required *EW*s for later use: TAME (Kang & Lee 2012).

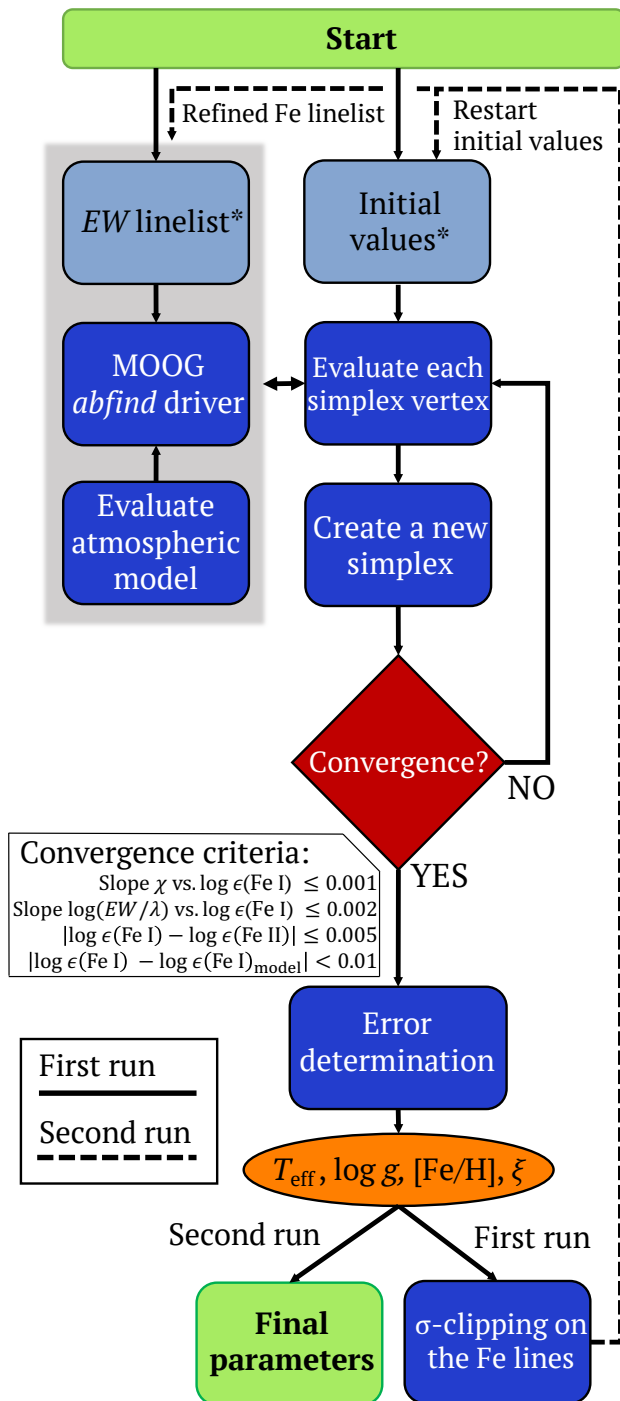


Fig. 1. STEPAR workflow diagram. As explained in Sect. 2.1, for any given star under analysis, the code performs two simplex runs. During the second simplex run, the initial values, which are initially set to the solar canonical values, are reset to the values obtained during the first run. Likewise, the *EW* linelist is refined according to the σ -clipping procedure on the Fe I lines. After the second run, the code halts execution and yields the final solution for the star.

- (v) An optimization algorithm: the Downhill Simplex method (Press et al. 2002).

2.1. STEPAR workflow

The stellar atmospheric parameters of FGK-type stars, namely T_{eff} , $\log g$, ξ , and $[\text{Fe}/\text{H}]$, can be derived in an automated fashion with STEPAR¹. Its workflow is shown in Fig. 1. In the standard STEPAR version presented here, we employed the 2017 version of the MOOG code (via the `abfind` driver, see Sneden 1973) and a grid of plane-parallel and spherical MARCS model atmospheres (Gustafsson et al. 2008), although other model grids can be used alongside STEPAR (see Tabernero et al. 2012, 2017; Montes et al. 2018). For lower gravities ($\log g < 3.5$) we used the spherical grid, whereas we employed the non-spherical grid for greater gravities ($\log g \geq 3.5$). Although MOOG treats the MARCS spherical atmospheric models as if they were plane-parallel, Heiter & Eriksson (2006) proved that this potential inconsistency is negligible. However, since the MARCS grid is finite, STEPAR includes an interpolation subroutine, based on the Python Scipy library, which draws on prior knowledge of the desired model and its neighbouring grid models to interpolate between them (Barber et al. 1996).

STEPAR needs a MOOG-compliant *EW* file as input, which can be provided by the user in the proper format using an automatic measurement tool. This MOOG-input file must contain the following atomic data for each line considered in the analysis:

- (i) Central wavelength of the line, in \AA ;
- (ii) A number that indicates the atomic number and ionisation stage of the chemical species that causes the line (26.0 and 26.1 in the case of Fe I and Fe II lines, respectively);
- (iii) the excitation potential, χ , in eV;
- (iv) the oscillator strength, $\log gf$;
- (v) the *EW* of the line in m \AA .

To perform our analysis we opted for the automatic code TAME² (Kang & Lee 2012), which can be run in either an automated or manual mode. Its manual mode has an interface that allows some user control over the *EW* measurements to check problematic spectra when needed. We followed the approach of Kang & Lee (2012) to adjust the `rejt` parameter of TAME according to the *S/N* of each spectrum. The other TAME parameters we employed were:

- (i) `smoother` = 4, the recommended parameter for smoothing the derivatives used for line identification;
- (ii) `space` = 3, the wavelength interval, in \AA , from each side of the central line to perform the *EW* computation;
- (iii) `lineresol` = 0.1, the minimum distance, in \AA , between two lines for TAME to resolve them;
- (iv) `miniline` = 2, the minimum *EW* that will be printed in the output.

Further details on TAME parameters can be found in Kang & Lee (2012). In addition, we only considered measured lines with $10 \text{ m\AA} < EW < 120 \text{ m\AA}$ to avoid problems with line profiles of very intense lines and tentatively bad *EW* measurements of extremely weak lines. For benchmark stars that have two high signal-to-noise spectra available, we applied an additional filter on the Fe I, II lines and rejected the ones that might have a differential equivalent width beyond three times the standard deviation of the *EW* differences between the corresponding Fe I, II lines measured on each of those two spectra.

¹ STEPAR is available at <https://github.com/hmtabernero/StePar> under the two-clause BSD license.

² TAME can be downloaded from <http://astro.snu.ac.kr/~wskang/tame/>

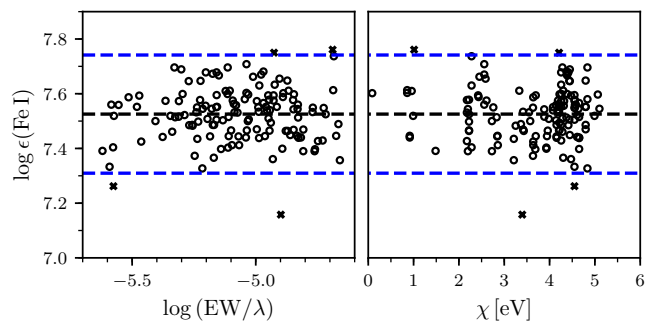


Fig. 2. STEPAR inner 3σ -clipping of the Fe I lines on the NARVAL spectrum of the Sun. $\log \epsilon(\text{Fe I})$ stands for the Fe abundance returned by the Fe lines while $\log(EW/\lambda)$ represents their reduced *EW*s. Black crosses depict the rejected Fe I lines. The dashed black lines represent a linear fit to the points, whereas the dashed blue lines are located at the 3σ -level.

As damping prescription, we used the Anstee-Barcklem-O'Mara (ABO, see Barklem et al. 1998) data (if available), through option 1 of MOOG. The atmospheric parameters can then be inferred from previously assembled Fe I-Fe II line lists.

The minimisation procedure of STEPAR is the Downhill Simplex algorithm (Press et al. 2002), which tries to minimise a quadratic form composed of the excitation and ionization equilibrium conditions to find the best parameters of the target star. This minimisation algorithm can reach convergence in very few iterations, and it is so fast that it is, for instance, the optimization method of choice for the ASCAP pipeline in APOGEE (Dawson et al. 2013). Since it does not use derivatives, they have to be estimated numerically, such as in the Levenberg-Marquardt method. If we let $\log \epsilon(\text{Fe I})$, and $\log \epsilon(\text{Fe II})$ stand for the Fe abundance returned by the Fe I and Fe II lines, respectively, and $\log(EW/\lambda)$ be their reduced equivalent width, STEPAR iterates until the slopes of χ versus $\log \epsilon(\text{Fe I})$ and $\log(EW/\lambda)$ versus $\log \epsilon(\text{Fe I})$ are virtually zero, i.e. excitation equilibrium, and imposing ionization equilibrium, so that $\log \epsilon(\text{Fe I}) = \log \epsilon(\text{Fe II})$. Throughout this procedure, we checked that the $[\text{Fe}/\text{H}]$ obtained from the iron lines is always compatible with the metallicity of the input atmospheric model. The actual convergence criteria of STEPAR, as shown in Fig. 1, are the following:

- (i) Slope ξ vs. $\log \epsilon(\text{Fe I}) \leq 0.001$;
- (ii) Slope $\log EW/\lambda$ vs. $\log \epsilon(\text{Fe I}) \leq 0.002$;
- (iii) $|\log \epsilon(\text{Fe I}) - \log \epsilon(\text{Fe II})| \leq 0.005$;
- (iv) $|\log \epsilon(\text{Fe I}) - \log \epsilon(\text{Fe I})_{\text{model}}| < 0.01$.

For each target spectrum, STEPAR performs two simplex runs, which in turn individually entail a full parameter determination using the Downhill Simplex optimization method. The first run deals with the *EW*s file as initially measured by TAME. Next, the best model that is found in this first run by the optimization routine is evaluated. STEPAR then performs a 3σ -clipping procedure on the Fe I abundance values obtained from the Fe I lines, so that we can remove the outliers, if any, due to "wrong" *EW*s measurements that could potentially invalidate the analysis. The second run is finally launched on a new input *EW* file that does not contain the rejected lines. An example of this 3σ -clipping procedure is shown in Fig. 2. As to execution time, STEPAR takes between 2 and 5 minutes to perform this whole procedure per star, depending on its actual position in the FGK parameter space.

To feed this minimisation process, the canonical solar values are used as initial input values ($T_{\text{eff}} = 5777 \text{ K}$, $\log g = 4.44 \text{ dex}$, $\xi = 1 \text{ km s}^{-1}$). However, STEPAR is able to reach a solution

even if the problem star is different from the Sun (e.g. a metal-poor giant). In other words, the final solution for any given star is independent of the initial set of parameters employed.

Finally, the uncertainties in the stellar parameters are determined as follows:

- (i) For the micro-turbulence, we slightly change the value of ξ until the slope of $\log \epsilon(\text{Fe I})$ vs. $\log (EW/\lambda)$ varies within its own error, divided by the square root of the number of Fe I lines.
- (ii) The effective temperature is varied until the slope of $\log \epsilon(\text{Fe I})$ vs. χ increases up to the error on the slope, divided by the square root of the number of Fe I lines. By increasing ξ on its error, we recompute the effective temperature. These two sources of error are added in quadrature.
- (iii) The surface gravity is then varied until the Fe II abundance increases by a quantity equal to the standard deviation divided by the square root of the number of Fe II lines. All the previous errors in ξ and T_{eff} are taken into account by varying these quantities separately, thus recomputing the gravity. These differences are later added in quadrature.
- (iv) Finally, to determine the error in the Fe abundance, the stellar atmospheric parameters are varied in their respective uncertainties, which enables the combination of all the Fe I, II variations due to the stellar parameters uncertainties and the standard deviation of the Fe I, II abundances in quadrature.

3. Testing the code

3.1. Selection of the Fe I, II linelists

The *EW* method requires a significantly large selection of reliable Fe I and Fe II lines. In principle, reliable lines are meant to be clean spectral lines that are not strongly affected by line blending of neighbouring lines or conspicuous spectral features. All the same, the available atomic data of these clean lines may not be precise enough for a trustworthy analysis. The main problem stems from the tabulated values of the transition probability per unit time of the spectral lines, $\log gf$. Some authors avoid this problem by calibrating this value for each line (see e.g. Santos et al. 2004; Sousa et al. 2008; Neves et al. 2009), normally by means of an inverse solar analysis, in which they vary the $\log gf$ value for a given line until they recover the corresponding solar abundance value. These are called the astrophysical $\log gf$ s.

The Gaia-ESO linelist (Heiter et al. 2015b) was originally extracted from a variety of sources with the aim of finding the best atomic parameters available. It contains around 560 Fe I, II features whose parameters were mostly taken from the Vienna Atomic Line Database (VALD³, Ryabchikova et al. 2015). The prime goal was to compile a trustworthy selection of lines to compute high-precision stellar parameters.

However, given the diversity of stars across the Milky Way (metal-poor dwarfs and giants, solar-type stars, metal rich giants, etc.) in the Gaia-ESO Survey, it soon became apparent that one linelist may fall short for the analysis of any given star. Hence, the analysis of any stellar sample under STEPAR is set to rely on four template stars from which four different lists of Fe I, II lines are assembled: the Sun, HD 22879, ξ Hya, and Arcturus. The corresponding linelists of Fe I and Fe II can be found in Table A.3 and Table A.4, respectively. These four template stars, which fully cover the FGK parameter space, as explained below, help us classify any star prior to the analysis with STEPAR.

Table 1. Linelist template stars and their reference stellar atmospheric parameters from Heiter et al. (2015a), with updated values from Jofré et al. (2018).

Star	List	T_{eff} [K]	$\log g$ [dex]	[Fe/H] [dex]
Sun	MRD	5777 ± 1	4.44 ± 0.01	0.03 ± 0.01
HD 22879	MPD	5868 ± 89	4.27 ± 0.03	-0.86 ± 0.05
ξ Hya	MRG	5044 ± 40	2.87 ± 0.02	0.16 ± 0.20
Arcturus	MPG	4286 ± 35	1.60 ± 0.20	-0.52 ± 0.08

Such division of the parameter space meets the following criteria. In terms of metallicity, we distinguish between metal-rich stars, i. e. $[\text{Fe}/\text{H}] \geq -0.30$, and metal-poor stars, i. e. $-0.30 > [\text{Fe}/\text{H}] \geq -1.50$. In terms of surface gravity, we make a distinction between the giant regime, i. e. $\log g < 4.00$, and the dwarf regime, i. e. $\log g \geq 4.00$. These partitions mean that the global parameter space is divided into four different regions: metal-rich dwarfs (MRD), metal-poor dwarfs (MPD), metal-rich giants (MRG), and metal-poor giants (MPG). Because of their scarcity, we decided to set aside the extremely metal-poor stars with $[\text{Fe}/\text{H}] < -1.50$. The general scheme of this division (MRD, MPD, MRG, MPG) is shown in Table 1.

As already mentioned, the analysis of any given star is done blindly, that is, its stellar parameters are not known beforehand. Hence, it is not known a priori which linelist corresponds to any given star. In order to overcome this issue, we measured the lines from all four linelists and did a first-pass with STEPAR so we could finally assign a linelist to each star depending on the parameters obtained. This preliminary step allowed us to run STEPAR with the corresponding linelist to get the final solution for the star.

3.2. Gaia benchmark test

Every spectroscopic study requires a reference point to assess the validity of the obtained results. Despite the Sun being widely used in the literature as a common reference, the use of one single star as a central point of reference provides no evidence on how a given method works in different regions of the parameter space.

In this regard, the Gaia benchmark stars were originally meant as calibrators to test the different approaches to the analysis. The availability of specific information for these stars was the key to determining their stellar atmospheric parameters independently from spectroscopy (Heiter et al. 2015a). In this sense, the Gaia benchmark stars represent a cornerstone when it comes to weighing the impact of the general limitations (e.g. wavelength coverage, linelists employed, resolution, etc.) inherent to any spectroscopic method that aims at the computation of such parameters.

Ideally, with a common background, any set of tools using the same data should converge to the same atmospheric parameters. However, the fact that every method takes into account a different set of spectral lines inevitably leads to slightly different stellar parameters. Although, in general, these differences are mostly dependent on the radiative transfer code, the stellar atmospheric models, the specific method, and the input data, among the GES nodes this dependence mostly comes down to the input data (i.e. measurement of *EW*s, signal-to-noise ratio of the spectra, the local continuum normalisation, etc.) and the method that each node takes into consideration.

³ <http://www.astro.uu.se/~vald/>

Table 2. Number of Fe I and Fe II in each of the four linelists used in this work. The wavelength coverage of all four lists is 4800–6800 Å, in line with that of the spectra under analysis. We also display the number of stars in each category.

Element	MRD	MPD	MRG	MPG
Fe I	146	127	113	115
Fe II	12	13	11	6
#stars	8	4	7	4

Table 3. Summary of the Montecarlo simulations performed using the stellar atmospheric parameters calculated in Sect. 3. Hereby we present the average difference on each parameter, along with the values of the Pearson (r_p) and the Spearman (r_s) correlation coefficients.

Parameter	Difference	r_p	r_s
T_{eff} [K]	9 ± 120	-0.12 ± 0.10	-0.15 ± 0.10
$\log g$ [dex]	-0.04 ± 0.30	-0.33 ± 0.16	-0.26 ± 0.14
[Fe/H] [dex]	0.05 ± 0.09	0.25 ± 0.10	0.16 ± 0.11

These stars, 23 in total, were taken from the stellar library⁴ described in Blanco-Cuaresma et al. (2014b), which covers the optical region 4800–6800 Å. The stars span a wide range in the parameter space (Heiter et al. 2015a; Jofré et al. 2015) that allowed us to test the reliability of the results given by STEPAR (see Table A.1). The internal consistency of the code was tested by deriving stellar atmospheric parameters from one or two high signal-to-noise spectra of the same star (see Table A.2).

4. Discussion

Although different spectra of the same object should theoretically result in exactly the same stellar atmospheric parameters, we noticed slight deviations in our analysis. The mean differences for the benchmark stars are 9 ± 32 K in T_{eff} , 0.00 ± 0.07 dex in $\log g$, and 0.00 ± 0.03 dex in [Fe/H].

These internal differences are mostly due to the quality of the individual spectra. The average uncertainties for the benchmark stars are 75 K in T_{eff} , 0.21 dex in $\log g$, and 0.06 dex in [Fe/H]. Furthermore, the average uncertainties are greater than the scatter that arises from the analysis of different spectra of the same object, as expected. Other sources of uncertainty might arise from systematic effects inherent to any methodology.

We compared the values of the stellar parameters for each spectrum to the reference values, as shown in Fig. 3. We found the following differences, all of which might be systematic: $\Delta T_{\text{eff}} = 9 \pm 89$ K, $\Delta \log g = -0.04 \pm 0.18$ dex, and $\Delta[\text{Fe}/\text{H}] = 0.05 \pm 0.06$ dex. At first glance, there are no notable differences at the 1-2 σ level. Additionally, in Fig. 4 we plot the line iron abundance retrieved by STEPAR for the final solution of the four reference stars.

However, since systematic trends may still remain hidden, we performed 10,000 Monte Carlo simulations on our data (as in Tabernero et al. 2018) in the hope of assessing possible sources of tentatively systematic offsets. We took each atmospheric parameter (T_{eff} , $\log g$, and [Fe/H]) to check any possible correlations by means of the Pearson and Spearman correlation coefficients, which are a measure of the correlation between any two given variables. Specifically, the Pearson coefficient is a classical correlation indicator, whereas the Spearman coefficient is a

⁴ The spectra of these stars can be downloaded from <https://www.blancocuaresma.com/s/benchmarkstars>

Table 4. Same differences as shown in Table 3 organised on a per-linelist basis, i.e. MRD, MPD, MRG, and MPG lists.

List	Difference		
	T_{eff} [K]	$\log g$ [dex]	[Fe/H] [dex]
MRD	14 ± 105	0.05 ± 0.19	0.06 ± 0.07
MPD	-88 ± 96	0.16 ± 0.18	0.03 ± 0.06
MRG	44 ± 122	0.05 ± 0.36	0.08 ± 0.08
MPG	28 ± 92	0.15 ± 0.31	0.05 ± 0.09

more robust non-parametric estimator of the statistical dependence of any two given variables (for more details, see e.g. Press et al. 2002). In Table 3 we clearly show that no systematic trends are present above the 2 σ level (i.e. within 95% confidence interval). These results are shown in Fig. 3 and Fig. A.1. Interestingly enough, even if the offsets in effective temperature and surface gravity are noticeable, the offset in the iron abundance is negligible (see Fig. 3). This is probably due to the fact that STEPAR produces self-consistent stellar parameters. For example, a deviation on the effective temperature can be compensated by the other parameters.

Finally, we assessed the performance of STEPAR in different regions of the parameter space. In Fig. 5 we plot a Kiel diagram, i.e. $\log g$ vs. $\log T_{\text{eff}}$, including the latest state-of-the-art YAPSI isochrones (Spada et al. 2017). In light of this figure, we do not find any major inconsistencies with the parameter space encompassed by the isochrones in general terms. However, we must notice that our method does not reproduce the gravity of K-stars, as they should have higher values. The former result is not entirely unexpected (Tabernero et al. 2012), as this result might be due to an ionization imbalance problem (Tsantaki et al. 2019). We still find higher effective temperatures for the F-type dwarfs, although they deviate less than in previous works (i.e. Tabernero et al. 2017; Montes et al. 2018). Finally, in Table 4 we show how STEPAR performs equally well in the four regions of the FGK parameter space defined in this work, i.e., MRD, MPD, MRG, and MPG, although the MRD and MPD linelists produce slightly larger errors than the rest. Interestingly enough, the errors in surface gravity are larger in the giant regime compared with the dwarf regime. As to the metallicity, we find a similar scatter in the four regions. Despite these differences, we find a good agreement with the reference values.

5. Conclusions

In this work, we have presented a robust code, STEPAR, which will hopefully be useful to the community when deriving the stellar atmospheric parameters of FGK-type stars under the *EW* method. This code has already been tested during the last few years against myriads of Gaia-ESO high-resolution spectra. We have also tested STEPAR against a library of Gaia Benchmark stars. Although we find some differences with the reference parameters, they are not significant.

Finally, we want to address some general limitations of the *EW* method that should be taken into consideration when using STEPAR. First, data must have enough quality to be analysed. This means that, since low signal-to-noise ratios (SNR) may translate into poor *EW* measurements, we highly recommend placing a cut at $\text{SNR} < 20$. In addition, we underline the importance of placing a lower limit in spectral resolution at $R = 30,000$ to prevent undesired line blending and suboptimal placement of the continuum level (Freeman & Bland-Hawthorn 2002). Sec-

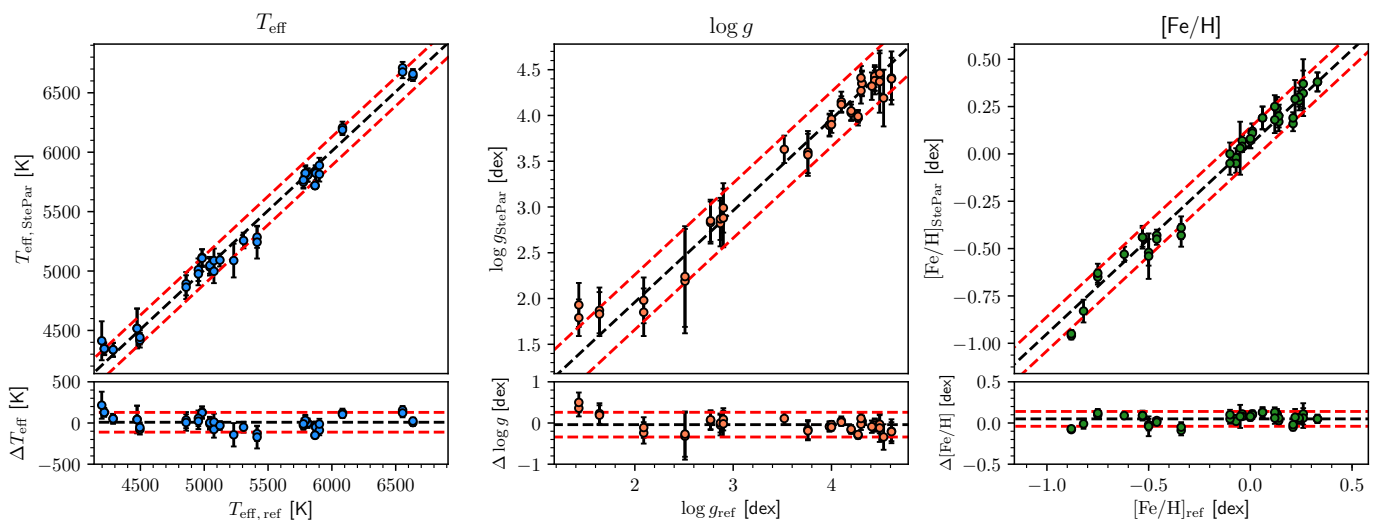


Fig. 3. STEPAR results for the Gaia benchmark stars plotted against the literature values taken from Heiter et al. (2015a), with updated values from Jofré et al. (2018). The upper panels show a one-to-one correspondence whereas the bottom panels depict the absolute differences. According to the values shown in Tab. 3, dashed black lines in the upper panels correspond to a one-to-one relationship, shifted following the average differences in each parameter, whereas in the bottom panels, they are centered at the average differences. The dashed red lines in all panels correspond to a margin of 120 K, 0.30 dex and 0.09 dex in T_{eff} , $\log g$ and $[\text{Fe}/\text{H}]$, respectively, according to the σ values found in the differences in each parameter.

ond, STEPAR cannot derive stellar atmospheric parameters of fast-rotating stars. Although the EW s are not, in fact, altered by rotation, the line profiles are indeed affected by rotational broadening and may no longer fit a Gaussian profile properly. In this sense, blending of neighbouring lines to the one of interest can also make it nearly impossible to get a reliable EW estimate for a given line. In these cases, we advise against using STEPAR on any star with a rotational velocity higher than 15 km s^{-1} . In addition, double-lined spectroscopic binaries should also be removed from any sample to avoid obtaining unreliable parameters. Finally, we do not recommend to derive stellar parameters with STEPAR for stars earlier than F6 and later than K4.

Acknowledgements. We would like to thank the anonymous referee for their insightful comments and suggestions to improve the manuscript of the paper. The authors acknowledge financial support from the Spanish Ministerio de Ciencia, Innovación y Universidades through projects AYA2016-79425-C3-1 (UCM), AYA2016-79425-C3-2 (CAB), and AYA2017-86389-P (IAC). E. M. acknowledges financial support from the Spanish Ministerio de Educación y Formación Profesional through fellowship FPU15/01476. J. I. G. H. also acknowledges financial support from the Spanish MINECO (Ministry of Economy of Spain) under the 2013 Ramón y Cajal programme MINECO RyC-2013-14875.

References

- Allende Prieto, C. 2016, *Living Reviews in Solar Physics*, 13, 1
- Allende Prieto, C., Beers, T. C., Wilhelm, R., et al. 2006, *ApJ*, 636, 804
- Andreasen, D. T., Sousa, S. G., Tsantaki, M., et al. 2017, *A&A*, 600, A69
- Barber, C. B., Dobkin, D. P., & Huhdanpaa, H. T. 1996, *ACM Trans. on Mathematical Software*, 22, 469
- Barklem, P. S., Anstee, S. D., & O’Mara, B. J. 1998, *PASA*, 15, 336
- Blanco-Cuaresma, S. 2019, *MNRAS*, 486, 2075
- Blanco-Cuaresma, S., Soubiran, C., Heiter, U., & Jofré, P. 2014a, *A&A*, 569, A111
- Blanco-Cuaresma, S., Soubiran, C., Jofré, P., & Heiter, U. 2014b, *A&A*, 566, A98
- Dalton, G., Trager, S., Abrams, D. C., et al. 2018, in *Society of Photo-Optical Instrumentation Engineers (SPIE) Conference Series*, Vol. 10702, Ground-based and Airborne Instrumentation for Astronomy VII, 107021B
- Dawson, K. S., Schlegel, D. J., Ahn, C. P., et al. 2013, *AJ*, 145, 10
- De Silva, G. M., Freeman, K. C., Bland-Hawthorn, J., et al. 2015, *MNRAS*, 449, 2604
- Deng, L.-C., Newberg, H. J., Liu, C., et al. 2012, *Research in Astronomy and Astrophysics*, 12, 735
- Freeman, K. & Bland-Hawthorn, J. 2002, *ARA&A*, 40, 487
- García Pérez, A. E., Allende Prieto, C., Holtzman, J. A., et al. 2016, *AJ*, 151, 144
- Ghezzi, L., Cunha, K., Smith, V. V., et al. 2010, *ApJ*, 720, 1290
- Gilmore, G., Randich, S., Asplund, M., et al. 2012, *The Messenger*, 147, 25
- González Hernández, J. I., Rebolo, R., Israelian, G., et al. 2004, *ApJ*, 609, 988
- González Hernández, J. I., Ruiz-Lapuente, P., Tabernero, H. M., et al. 2012, *Nature*, 489, 533
- Gustafsson, B., Edvardsson, B., Eriksson, K., et al. 2008, *A&A*, 486, 951
- Heiter, U. & Eriksson, K. 2006, *A&A*, 452, 1039
- Heiter, U., Jofré, P., Gustafsson, B., et al. 2015a, *A&A*, 582, A49
- Heiter, U., Lind, K., Asplund, M., et al. 2015b, *Phys. Scr*, 90, 054010
- Hekker, S. & Meléndez, J. 2007, *A&A*, 475, 1003
- Hubeny, I. & Mihalas, D. 2014, *Theory of Stellar Atmospheres* (Princeton University Press)
- Jofré, P., Heiter, U., & Soubiran, C. 2018, arXiv e-prints [arXiv:1811.08041]
- Jofré, P., Heiter, U., Soubiran, C., et al. 2015, *A&A*, 582, A81
- Jofré, P., Heiter, U., Worley, C. C., et al. 2017, *A&A*, 601, A38
- Kang, W. & Lee, S.-G. 2012, *MNRAS*, 425, 3162
- Kunder, A., Kordopatis, G., Steinmetz, M., et al. 2017, *AJ*, 153, 75
- Lanzafame, A. C., Frasca, A., Damiani, F., et al. 2015, *A&A*, 576, A80
- Lee, Y. S., Beers, T. C., Sivarani, T., et al. 2008, *AJ*, 136, 2022
- Magrini, L., Randich, S., Friel, E., et al. 2013, *A&A*, 558, A38
- Masseron, T., Merle, T., & Hawkins, K. 2016, BACCHUS: Brussels Automatic Code for Characterizing High accuracy Spectra, Astrophysics Source Code Library
- Montes, D., González-Peinado, R., Tabernero, H. M., et al. 2018, *MNRAS*, 479, 1332
- Mucciarelli, A., Pancino, E., Lovisi, L., Ferraro, F. R., & Lapenna, E. 2013, *ApJ*, 766, 78
- Neves, V., Santos, N. C., Sousa, S. G., Correia, A. C. M., & Israelian, G. 2009, *A&A*, 497, 563
- Nissen, P. E. & Gustafsson, B. 2018, *A&A Rev.*, 26, 6
- Piskunov, N. & Valenti, J. A. 2017, *A&A*, 597, A16
- Press, W. H., Teukolsky, S. A., Vetterling, W. T., & Flannery, B. P. 2002, *Numerical recipes in C++: the art of scientific computing* (Cambridge University Press)
- Ryabchikova, T., Piskunov, N., Kurucz, R. L., et al. 2015, *Phys. Scr*, 90, 054005
- Santos, N. C., Israelian, G., & Mayor, M. 2004, *A&A*, 415, 1153
- Smiljanic, R., Korn, A. J., Bergemann, M., et al. 2014, *A&A*, 570, A122
- Snedden, C. 1973, *ApJ*, 184, 839
- Soto, M. G. & Jenkins, J. S. 2018, *A&A*, 615, A76
- Sousa, S. G., Santos, N. C., Israelian, G., Mayor, M., & Monteiro, M. J. P. F. G. 2007, *A&A*, 469, 783
- Sousa, S. G., Santos, N. C., Mayor, M., et al. 2008, *A&A*, 487, 373
- Spada, F., Demarque, P., Kim, Y. C., Boyajian, T. S., & Brewer, J. M. 2017, *ApJ*, 838, 161
- Stetson, P. B. & Pancino, E. 2008, *PASP*, 120, 1332

- Taberero, H. M. 2014, PhD thesis, Departamento de Astrofísica, Facultad de Ciencias Físicas, Universidad Complutense de Madrid, 28040 Madrid, Spain
- Taberero, H. M., Dorda, R., Negueruela, I., & González-Fernández, C. 2018, *MNRAS*, 476, 3106
- Taberero, H. M., Montes, D., & González Hernández, J. I. 2012, *A&A*, 547, A13
- Taberero, H. M., Montes, D., González Hernández, J. I., & Ammler-von Eiff, M. 2017, *A&A*, 597, A33
- Tsantaki, M., Andreasen, D. T., Teixeira, G. D. C., et al. 2018, *MNRAS*, 473, 5066
- Tsantaki, M., Santos, N. C., Sousa, S. G., et al. 2019, *MNRAS*, 569
- Tsantaki, M., Sousa, S. G., Adibekyan, V. Z., et al. 2013, *A&A*, 555, A150
- Tsantaki, M., Sousa, S. G., Santos, N. C., et al. 2014, *A&A*, 570, A80
- Valenti, J. A. & Piskunov, N. 1996, *A&AS*, 118, 595

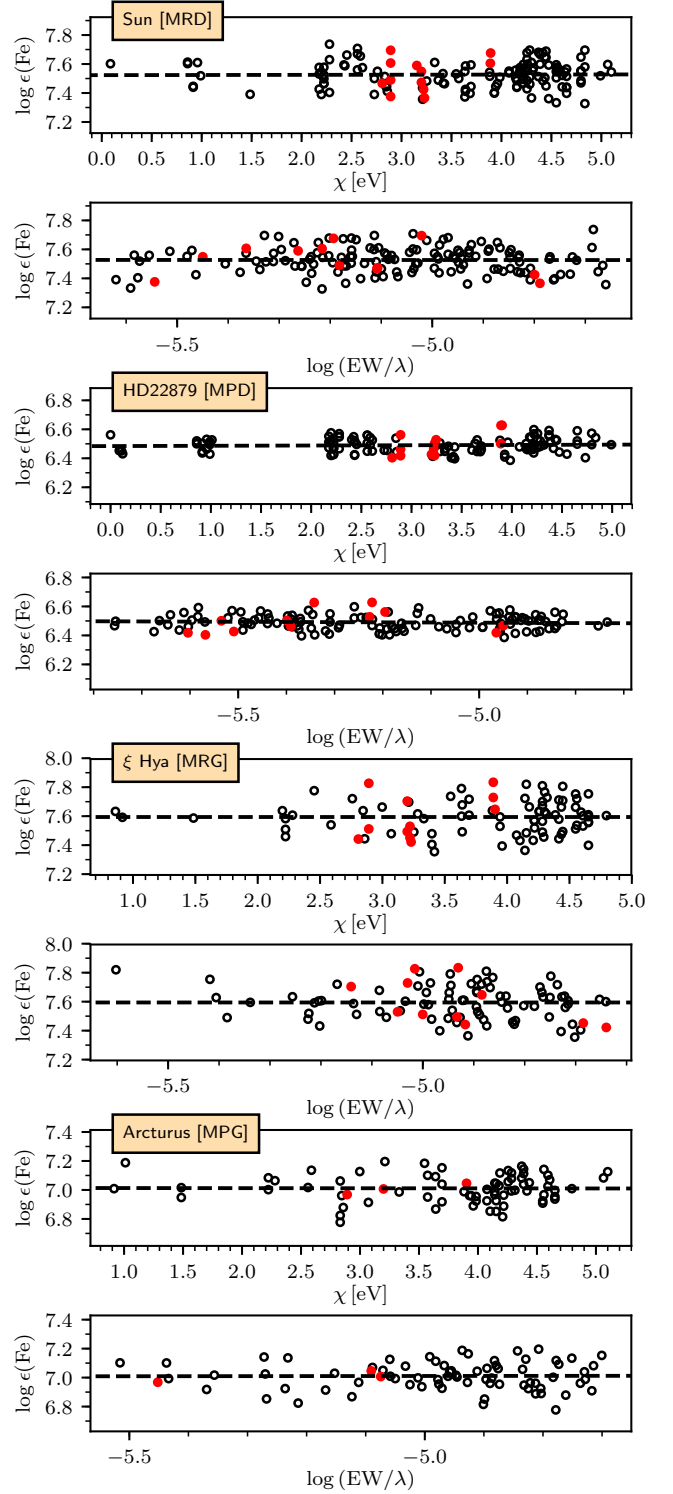


Fig. 4. From top to bottom: line iron abundance retrieved by STEPAR for the final solution of the four reference stars: the Sun (NARVAL), HD 22879 (NARVAL), ξ Hya (ESPaDOns) and Arcturus (UVES). $\log \epsilon(\text{Fe I})$ stands for the Fe abundance returned by the Fe lines while $\log(\text{EW}/\lambda)$ represents their reduced EWs. Unfilled black dots represent Fe I lines, whereas red dots depict Fe II lines. The dashed black lines represent the least-squares fit to the data points.

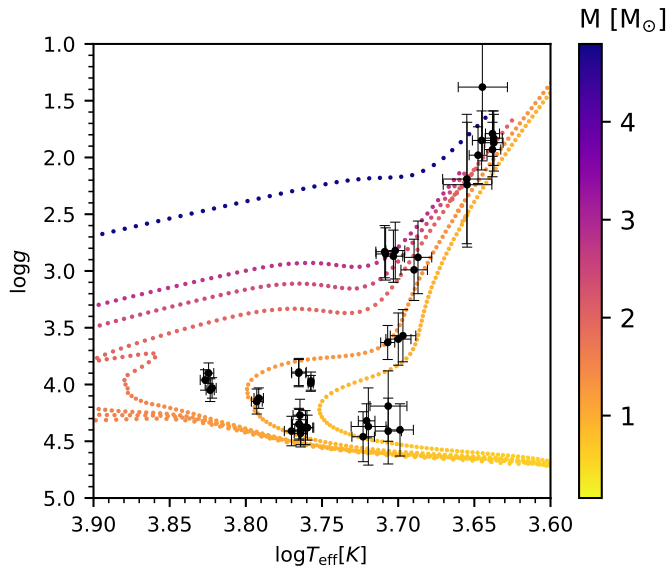


Fig. 5. Kiel diagram ($\log g$ vs. $\log T_{\text{eff}}$) for all the spectra alongside the YaPSI isochrones for 0.1, 0.4, 0.6, 1, 4, and 13 Ga (for $Z=0.016$, see Spada et al. 2017).

Appendix A: Appendix

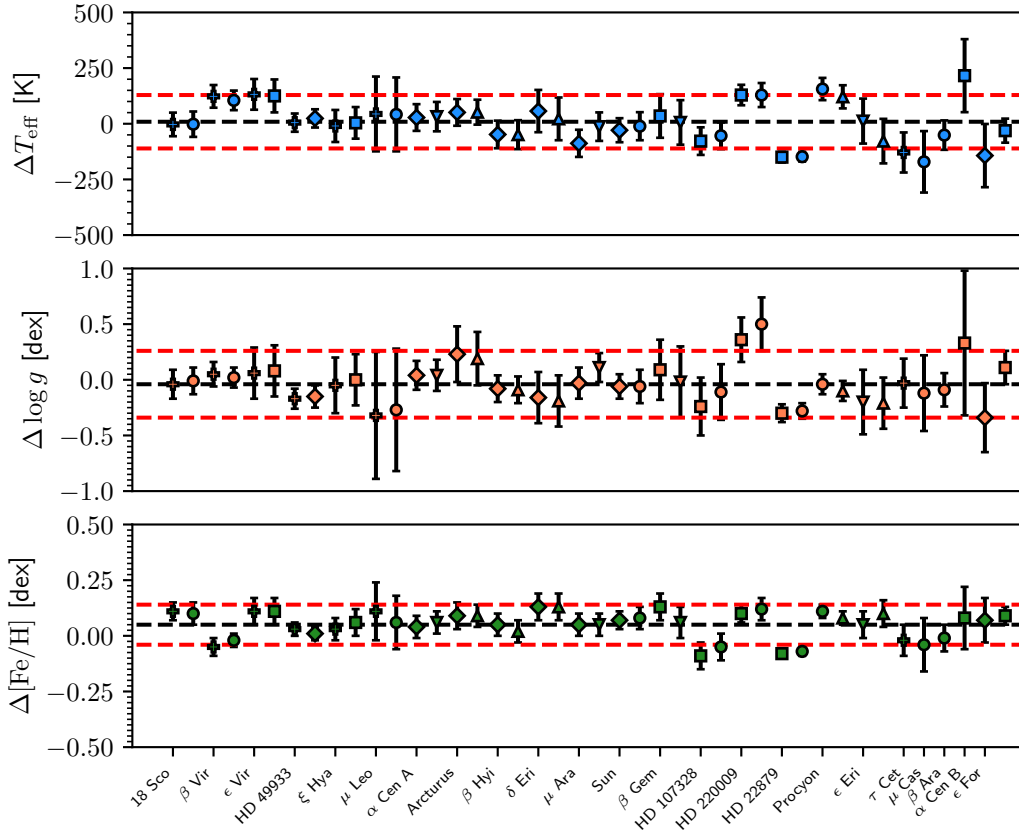


Fig. A.1. STEPAR differences with respect to the reference values (Heiter et al. 2015a) where each symbol denotes a different spectrograph: NARVAL (circles), HARPS.GBOG (squares), HARPS.Archive (diamonds), UVES.POP (upward triangles), UVES (downward triangles), ESPaDOnS (crosses).

Table A.1. Reference stellar atmospheric parameters of the Gaia benchmark stars taken from Heiter et al. (2015a), with updated values from Jofré et al. (2018).

Star	Spectral type	T_{eff} [K]	$\log g$ [dex]	[Fe/H] [dex]
Metal-rich dwarfs (MRD)				
Procyon	F5IV-V	6554 ± 84	4.00 ± 0.02	0.01 ± 0.08
β Vir	F9V	6083 ± 41	4.10 ± 0.02	0.24 ± 0.07
μ Ara	G3IV-V	5902 ± 66	4.30 ± 0.03	0.35 ± 0.13
18 Sco	G2Va	5810 ± 80	4.44 ± 0.03	0.03 ± 0.03
α Cen A	G2V	5792 ± 16	4.31 ± 0.01	0.26 ± 0.08
Sun	G2V	5771 ± 1	4.44 ± 0.00	0.03 ± 0.05
α Cen B	K1V	5231 ± 20	4.53 ± 0.03	0.22 ± 0.10
ϵ Eri	K2Vk:	5076 ± 30	4.61 ± 0.03	-0.09 ± 0.06
Metal-poor dwarfs (MPD)				
HD 49933	F2V	6635 ± 91	4.20 ± 0.03	-0.41 ± 0.08
HD 22879	F9V	5868 ± 89	4.27 ± 0.04	-0.86 ± 0.05
τ Cet	G8.5V	5414 ± 21	4.49 ± 0.02	-0.49 ± 0.03
μ Cas	G5Vb	5308 ± 29	4.41 ± 0.06	-0.81 ± 0.03
Metal-rich giants (MRG)				
β Hyi	G0V	5873 ± 45	3.98 ± 0.02	-0.04 ± 0.06
ξ Hya	G7III	5044 ± 40	2.87 ± 0.02	0.16 ± 0.20
ϵ Vir	G8III	4983 ± 61	2.77 ± 0.02	0.15 ± 0.16
δ Eri	K1III-IV	4954 ± 30	3.76 ± 0.02	0.06 ± 0.05
β Gem	K0IIIb	4858 ± 60	2.90 ± 0.08	0.13 ± 0.16
μ Leo	K2III	4474 ± 60	2.51 ± 0.11	0.25 ± 0.15
β Ara	K3Ib-II	4197 ± 50	1.05 ± 0.15	-0.05 ± 0.39
Metal-poor dwarfs (MPG)				
ϵ For	K2V*	5123 ± 78	3.52 ± 0.08	-0.60 ± 0.10
HD 107328	K0IIIb	4496 ± 59	2.09 ± 0.13	-0.33 ± 0.16
Arcturus	K1.5III	4286 ± 35	1.60 ± 0.20	-0.52 ± 0.08
HD 220009	K2III	4217 ± 60	1.43 ± 0.12	-0.74 ± 0.13

Table A.2. STEPAR results.

Star	Spectral type	Source	SNR	T_{eff} [K]	ΔT_{eff} [K]	$\log g$ [dex]	$\Delta \log g$ [dex]	ξ_{micro} [km s ⁻¹]	$\Delta \xi_{\text{micro}}$ [km s ⁻¹]	[Fe/H] [dex]	Δ [Fe/H] [dex]
Metal-rich dwarfs (MRD)											
Procyon	F5IV-V	NARVAL	765	6710	50	3.96	0.09	1.70	0.06	0.07	0.03
Procyon	F5IV-V	UVES.POP	1016	6675	52	3.90	0.09	1.63	0.06	0.04	0.03
β Vir	F9V	ESPaDOnS	635	6206	51	4.15	0.11	1.43	0.07	0.16	0.04
β Vir	F9V	NARVAL	400	6188	44	4.12	0.09	1.33	0.05	0.19	0.03
μ Ara	G3IV-V	HARPS.Archive	252	5814	61	4.27	0.14	0.95	0.09	0.38	0.05
μ Ara	G3IV-V	UVES	309	5889	64	4.41	0.13	1.03	0.10	0.38	0.05
18 Sco	G2Va	ESPaDOnS	383	5807	53	4.40	0.13	0.69	0.11	0.12	0.04
18 Sco	G2Va	NARVAL	380	5808	57	4.43	0.12	0.74	0.11	0.11	0.05
α Cen A	G2V	HARPS.Archive	496	5820	60	4.35	0.13	0.96	0.09	0.28	0.05
α Cen A	G2V	UVES	316	5824	66	4.35	0.14	0.86	0.11	0.30	0.05
Sun	G2V	HARPS.Archive	549	5748	54	4.38	0.11	0.62	0.12	0.07	0.04
Sun	G2V	NARVAL	828	5766	63	4.38	0.15	0.70	0.12	0.08	0.05
α Cen B	K1V	HARPS	469	5088	142	4.19	0.31	0.50	0.30	0.29	0.10
ϵ Eri	K2Vk:	UVES	220	5088	101	4.41	0.29	0.78	0.21	-0.05	0.06
ϵ Eri	K2Vk:	UVES.POP	1653	4998	100	4.40	0.23	0.41	0.28	0.00	0.06
Metal-poor dwarfs (MPD)											
HD 49933	F2V	HARPS.Archive	319	6659	41	4.05	0.10	1.54	0.05	-0.45	0.03
HD 49933	F2V	ESPaDOnS	1169	6640	41	4.03	0.09	1.56	0.05	-0.43	0.03
HD 22879	F9V	HARPS.GBOG	322	5718	24	3.97	0.08	1.04	0.03	-0.96	0.02
HD 22879	F9V	NARVAL	297	5720	22	3.99	0.07	1.02	0.03	-0.95	0.02
τ Cet	G8.5V	ESPaDOnS	1238	5285	90	4.46	0.22	0.43	0.21	-0.52	0.07
τ Cet	G8.5V	NARVAL	357	5243	138	4.37	0.34	0.50	0.35	-0.54	0.12
μ Cas	G5Vb	NARVAL	269	5257	66	4.32	0.15	0.42	0.24	-0.83	0.06
Metal-rich giants (MRG)											
β Hyi	G0V	HARPS.Archive	428	5825	62	3.90	0.12	0.84	0.08	-0.02	0.05
β Hyi	G0V	UVES.POP	676	5824	65	3.89	0.12	0.92	0.07	-0.05	0.05
ξ Hya	G7III	HARPS.GBOG	391	5048	71	2.87	0.23	1.17	0.07	0.20	0.06
ξ Hya	G7III	ESPaDOnS	526	5034	72	2.82	0.25	1.20	0.07	0.17	0.05
ϵ Vir	G8III	ESPaDOnS	435	5115	69	2.83	0.23	1.33	0.07	0.24	0.06
ϵ Vir	G8III	HARPS.GBOG	392	5108	74	2.85	0.23	1.33	0.07	0.24	0.06
δ Eri	K1III-IV	HARPS.Archive	525	5011	95	3.60	0.23	0.77	0.13	0.19	0.06
δ Eri	K1III-IV	UVES.POP	548	4976	96	3.57	0.23	0.72	0.14	0.19	0.06
β Gem	K0IIIb	HARPS.GBOG	370	4893	98	2.99	0.27	1.07	0.09	0.25	0.06
β Gem	K0IIIb	UVES	163	4864	100	2.88	0.32	1.14	0.10	0.18	0.07
μ Leo	K2III	ESPaDOnS	779	4518	168	2.19	0.57	1.25	0.12	0.37	0.13
μ Leo	K2III	NARVAL	402	4516	166	2.24	0.55	1.34	0.13	0.32	0.12
β Ara	K3Ib-II	HARPS.GBOG	414	4413	164	1.38	0.65	2.20	0.18	0.03	0.14
Metal-poor giants (MPD)											
ϵ For	K2V*	HARPS.GBOG	334	5092	54	3.63	0.15	0.70	0.10	-0.53	0.04
HD 107328	K0IIIb	HARPS.GBOG	459	4418	62	1.85	0.26	1.71	0.07	-0.43	0.06
HD 107328	K0IIIb	NARVAL	375	4442	60	1.98	0.25	1.68	0.06	-0.39	0.06
Arcturus	K1.5III	HARPS.Archive	475	4337	60	1.87	0.25	1.64	0.07	-0.44	0.06
Arcturus	K1.5III	UVES.POP	1208	4338	56	1.83	0.24	1.59	0.06	-0.44	0.05
HD 220009	K2III	HARPS.GBOG	347	4346	46	1.79	0.20	1.42	0.05	-0.65	0.04
HD 220009	K2III	NARVAL	376	4346	54	1.93	0.24	1.45	0.06	-0.63	0.05

Table A.3. Merged Fe I linelists.

λ_{air} [Å]	χ_1 [eV]	$\log gf$	List			
			MRD	MPD	MRG	MPG
4808.148	3.25	-2.690	•		•	
4809.938	3.57	-2.620	•			•
4869.463	3.55	-2.420	•		•	•
4875.877	3.33	-1.900	•	•		
4877.604	3.00	-3.050			•	•
4882.143	3.42	-1.480		•	•	
4892.859	4.22	-1.290	•	•	•	•
4903.310	2.88	-0.903			•	
4905.133	3.93	-1.730	•			
4907.732	3.43	-1.700	•	•		
4917.230	4.19	-1.080		•		
4924.770	2.28	-2.216	•	•		
4939.687	0.86	-3.336	•	•		•
4946.387	3.37	-1.110	•	•	•	•
4950.105	3.42	-1.490	•	•		
4961.913	3.63	-2.190	•			
4962.572	4.18	-1.182	•	•	•	
4966.088	3.33	-0.792	•	•		
4969.917	4.22	-0.710		•		
4985.253	3.93	-0.447		•		
4986.223	4.22	-1.290		•		
4992.785	4.26	-2.350			•	
4993.680	4.21	-1.370	•			
4994.130	0.92	-3.058	•	•	•	•
5002.792	3.40	-1.460	•	•	•	•
5012.695	4.28	-1.690	•		•	
5014.942	3.94	-0.183		•	•	•
5022.235	3.98	-0.370		•	•	
5023.186	4.28	-1.500			•	
5029.618	3.42	-1.950	•			
5031.914	4.37	-1.570				•
5044.211	2.85	-2.038	•	•	•	
5048.436	3.96	-1.005			•	
5049.820	2.28	-1.348		•	•	
5054.642	3.64	-1.921	•			•
5060.078	0.00	-5.431		•	•	
5067.150	4.22	-0.970	•	•		
5068.766	2.94	-1.041			•	
5074.748	4.22	-0.230		•	•	
5079.223	2.20	-2.068		•		
5079.740	0.99	-3.221		•		
5083.338	0.96	-2.939		•	•	
5088.153	4.15	-1.680				•
5090.773	4.26	-0.440	•	•		
5104.438	4.28	-1.590			•	
5107.447	0.99	-3.089		•		
5109.652	4.30	-0.980			•	
5127.359	0.92	-3.306		•		
5133.688	4.18	0.360		•	•	
5141.739	2.42	-1.978			•	•
5143.723	2.20	-3.690			•	
5150.839	0.99	-3.008		•	•	
5151.911	1.01	-3.322	•	•		
5159.058	4.28	-0.820		•		
5162.273	4.18	0.020		•		
5197.936	4.30	-1.540	•		•	
5198.711	2.22	-2.135	•	•	•	
5213.806	3.94	-2.760			•	

Table A.3. Merged Fe I linelists (cont.).

λ_{air} [Å]	χ_1 [eV]	$\log gf$	List			
			MRD	MPD	MRG	MPG
5215.180	3.27	-0.861			•	
5216.274	1.61	-2.082			•	
5217.389	3.21	-1.074	•	•	•	•
5225.526	0.11	-4.789		•		
5228.376	4.22	-1.190		•		
5229.845	3.28	-0.967		•		
5242.491	3.63	-0.967	•	•	•	•
5243.776	4.26	-1.050	•	•	•	•
5247.050	0.09	-4.949	•	•		
5250.209	0.12	-4.933		•		
5250.646	2.20	-2.180		•		
5253.462	3.28	-1.579		•	•	
5285.127	4.44	-1.660	•		•	•
5288.525	3.70	-1.493	•			•
5293.959	4.14	-1.770			•	•
5294.547	3.64	-2.760	•		•	
5295.312	4.42	-1.590	•		•	•
5307.361	1.61	-2.912	•	•		•
5321.108	4.44	-1.089				•
5322.041	2.28	-2.802	•			•
5339.929	3.27	-0.635				•
5364.871	4.45	0.228			•	•
5373.709	4.47	-0.710	•	•		
5379.574	3.70	-1.514	•	•	•	•
5386.333	4.15	-1.670	•		•	•
5389.479	4.42	-0.410		•	•	
5397.618	3.63	-2.528			•	
5398.279	4.45	-0.630	•	•	•	
5400.501	4.37	-0.160	•	•		
5401.266	4.32	-1.820	•		•	
5409.133	4.37	-1.200	•	•		
5417.033	4.42	-1.580	•		•	
5424.068	4.32	0.520		•		
5436.295	4.39	-1.440	•		•	•
5436.588	2.28	-2.964			•	
5441.339	4.31	-1.630	•		•	•
5445.042	4.39	-0.020		•	•	•
5460.873	3.07	-3.426			•	•
5461.550	4.45	-1.800	•		•	
5463.275	4.44	0.070			•	•
5464.280	4.14	-1.402			•	
5466.396	4.37	-0.630	•	•		•
5470.093	4.45	-1.710	•		•	
5472.709	4.21	-1.495	•			
5473.900	4.15	-0.720	•	•		
5483.099	4.15	-1.392	•			•
5501.465	0.96	-3.046		•		
5506.779	0.99	-2.795		•		
5522.446	4.21	-1.450	•	•		
5536.580	2.83	-3.710				•
5539.280	3.64	-2.560				•
5543.147	3.70	-1.470		•		
5543.936	4.22	-1.040	•	•	•	•
5546.506	4.37	-1.210		•		
5549.949	3.70	-2.810			•	
5554.894	4.55	-0.270		•		
5560.212	4.44	-1.090	•	•	•	
5572.842	3.40	-0.289				•
5576.089	3.43	-0.900		•	•	•

Table A.3. Merged Fe I linelists (cont.).

λ_{air} [Å]	χ_1 [eV]	$\log gf$	List			
			MRD	MPD	MRG	MPG
5618.632	4.21	-1.255	•	•	•	•
5619.595	4.39	-1.600	•			•
5633.946	4.99	-0.230		•		
5635.822	4.26	-1.790	•			
5636.696	3.64	-2.510	•		•	
5638.262	4.22	-0.720	•	•		
5641.434	4.26	-1.080	•	•		
5649.987	5.10	-0.820	•			•
5651.469	4.47	-1.900	•			
5652.318	4.26	-1.850	•			
5653.865	4.39	-1.540	•			•
5655.176	5.06	-0.600	•			•
5661.345	4.28	-1.756	•			•
5662.516	4.18	-0.447	•	•		•
5679.023	4.65	-0.820	•	•	•	•
5691.497	4.30	-1.450		•		
5696.089	4.55	-1.720	•			
5701.544	2.56	-2.193	•	•		
5705.464	4.30	-1.355	•			
5717.833	4.28	-0.990	•	•	•	•
5720.886	4.55	-1.631	•		•	•
5731.762	4.26	-1.200	•	•		•
5732.296	4.99	-1.460	•			
5741.848	4.26	-1.672	•			
5759.262	4.65	-2.216			•	
5778.453	2.59	-3.430			•	
5784.658	3.40	-2.547			•	
5844.918	4.15	-3.054			•	
5849.683	3.70	-2.890				•
5852.219	4.55	-1.230	•		•	
5853.148	1.49	-5.180			•	•
5855.076	4.61	-1.478	•		•	
5856.088	4.29	-1.327			•	
5858.778	4.22	-2.160			•	
5861.109	4.28	-2.304			•	•
5883.816	3.96	-1.260	•	•		•
5902.473	4.59	-1.710				•
5905.671	4.65	-0.690	•	•	•	•
5909.972	3.21	-2.587	•		•	•
5916.247	2.45	-2.994	•		•	•
5927.789	4.65	-0.990	•		•	
5929.676	4.55	-1.310	•		•	
5930.180	4.65	-0.230	•	•	•	
5934.654	3.93	-1.070	•	•		•
5940.991	4.18	-2.050				•
5952.718	3.98	-1.340				•
5956.694	0.86	-4.599	•	•	•	•
6003.011	3.88	-1.100	•	•	•	•
6012.210	2.22	-4.038				•
6019.365	3.57	-3.310				•
6024.057	4.55	-0.120	•	•		•
6027.051	4.08	-1.089	•	•	•	•
6056.005	4.73	-0.320		•		
6065.482	2.61	-1.529		•	•	
6079.008	4.65	-1.020	•	•	•	•
6082.710	2.22	-3.576	•		•	•
6093.643	4.61	-1.400	•		•	•
6094.373	4.65	-1.840				•
6096.664	3.98	-1.830	•			•

Table A.3. Merged Fe I linelists (cont.).

λ_{air} [Å]	χ_1 [eV]	$\log gf$	List			
			MRD	MPD	MRG	MPG
6098.244	4.56	-1.859	•		•	•
6120.246	0.92	-5.970			•	•
6127.906	4.14	-1.399	•	•		•
6136.615	2.45	-1.402		•		
6136.994	2.20	-2.950		•		
6137.691	2.59	-1.402		•		
6151.617	2.18	-3.295	•	•		•
6165.360	4.14	-1.473	•	•		•
6170.506	4.80	-0.440	•	•		
6173.334	2.22	-2.880	•	•	•	•
6180.203	2.73	-2.591	•			
6187.989	3.94	-1.620	•		•	•
6191.557	2.43	-1.416		•		
6199.506	2.56	-4.430				•
6200.312	2.61	-2.433	•	•		•
6213.429	2.22	-2.481	•	•		•
6219.280	2.20	-2.432	•	•		•
6220.780	3.88	-2.058				•
6226.734	3.88	-2.120	•			
6229.226	2.85	-2.805	•		•	•
6230.722	2.56	-1.281	•	•		
6240.646	2.22	-3.230	•	•	•	•
6246.318	3.60	-0.771	•	•	•	
6252.555	2.40	-1.699	•	•	•	•
6265.132	2.18	-2.550	•	•	•	•
6270.223	2.86	-2.470	•		•	•
6271.278	3.33	-2.703			•	•
6280.617	0.86	-4.390		•		
6290.543	2.59	-4.330				•
6297.793	2.22	-2.737		•		•
6301.500	3.65	-0.720		•	•	•
6311.499	2.83	-3.141	•			•
6315.811	4.08	-1.630	•			•
6322.685	2.59	-2.430	•	•	•	•
6335.330	2.20	-2.177	•	•	•	•
6336.823	3.69	-0.852	•	•	•	•
6338.876	4.80	-0.960	•			
6344.148	2.43	-2.919		•		
6355.028	2.85	-2.340		•		
6380.743	4.19	-1.375	•			•
6393.600	2.43	-1.452		•	•	
6400.317	0.92	-4.318	•	•		
6411.648	3.65	-0.596		•		
6421.350	2.28	-2.012	•	•		
6430.845	2.18	-2.005	•	•		
6469.192	4.84	-0.730	•	•		
6475.624	2.56	-2.941	•	•		
6481.870	2.28	-2.981	•	•		•
6494.980	2.40	-1.268		•		
6495.741	4.84	-0.840	•			
6496.466	4.80	-0.530	•	•		•
6498.938	0.96	-4.687	•			•
6518.366	2.83	-2.438				•
6533.928	4.56	-1.360	•	•	•	•
6546.238	2.76	-1.536		•	•	•
6574.227	0.99	-5.004	•			
6581.209	1.49	-4.679				•
6591.313	4.59	-2.081			•	•
6592.912	2.73	-1.473	•	•		•

Table A.3. Merged Fe I linelists (cont.).

λ_{air} [Å]	χ_1 [eV]	$\log gf$	List			
			MRD	MPD	MRG	MPG
6593.869	2.43	-2.420	•	•		•
6597.559	4.80	-0.970	•			•
6608.025	2.28	-3.930	•			•
6609.110	2.56	-2.691	•	•		•
6627.544	4.55	-1.590	•			
6633.412	4.84	-1.390	•			
6633.749	4.56	-0.799	•			
6648.080	1.01	-5.918				•
6703.566	2.76	-3.060	•		•	
6710.318	1.49	-4.764	•			
6713.743	4.80	-1.500	•		•	
6716.236	4.58	-1.836	•			
6725.356	4.10	-2.100			•	•
6750.151	2.42	-2.618	•	•	•	•
6752.707	4.64	-1.204	•			

Table A.4. Merged Fe II linelists.

λ_{air} [Å]	χ_1 [eV]	$\log gf$	List			
			MRD	MPD	MRG	MPG
4993.350	2.81	-3.684	•	•	•	
5197.568	3.23	-2.220	•	•	•	
5234.623	3.22	-2.180	•	•	•	•
5256.932	2.89	-4.182	•		•	
5264.802	3.23	-3.130		•		
5284.103	2.89	-3.195		•		
5325.552	3.22	-3.160		•		•
5414.070	3.22	-3.580			•	
5425.248	3.20	-3.220	•	•	•	•
5534.838	3.25	-2.865		•		
5991.371	3.15	-3.647	•			
6084.102	3.20	-3.881	•		•	
6149.246	3.89	-2.841	•		•	•
6238.386	3.89	-2.600		•	•	
6247.557	3.89	-2.435		•		
6369.459	2.89	-4.110	•			•
6416.919	3.89	-2.877	•			
6432.676	2.89	-3.570	•	•	•	
6456.380	3.90	-2.185		•	•	•
6516.077	2.89	-3.310	•	•		